

Wheel Transformer: A Wheel-Leg Hybrid Robot With Passive Transformable Wheels

Yoo-Seok Kim, *Student Member, IEEE*, Gwang-Pil Jung, *Student Member, IEEE*, Haan Kim, Kyu-Jin Cho, *Member, IEEE*, and Chong-Nam Chu

Abstract—We report on the design, optimization, and performance evaluation of a new wheel-leg hybrid robot. This robot utilizes a novel transformable wheel that combines the advantages of both circular and legged wheels. To minimize the complexity of the design, the transformation process of the wheel is passive, which eliminates the need for additional actuators. A new triggering mechanism is also employed to increase the transformation success rate. To maximize the climbing ability in legged-wheel mode, the design parameters for the transformable wheel and robot are tuned based on behavioral analyses. The performance of our new development is evaluated in terms of stability, energy efficiency, and the maximum height of an obstacle that the robot can climb over. With the new transformable wheel, the robot can climb over an obstacle 3.25 times as tall as its wheel radius, without compromising its driving ability at a speed of 2.4 body lengths/s with a specific resistance of 0.7 on a flat surface.

Index Terms—Legged robots, mechanism design, search and rescue (SAR) robots, transformable wheel, wheeled robots.

I. INTRODUCTION

SMALL mobile robots offer the advantage of being able to scout out areas that humans might find difficult to access, such as the narrow spaces within a collapsed building. In such situations, small mobile robots could be used in reconnaissance or search and rescue (SAR) missions [1], [2]. To date, ordinary circular wheels have been the most common method of locomotion because of their stability and efficiency on flat surfaces. At the same time, however, small mobile robots lose their ability to

climb over obstacles because the objects around them become relatively larger [3]. Specifically, a circular wheel cannot climb over obstacles taller than its radius, and is thus unsuitable for propelling a small robotic system through rough terrain.

Legged wheels were devised to overcome the limited climbing ability of circular wheels. Such wheels are rimless and have several spokes, which allow them to climb obstacles taller than their radius. A few different types of such legged-wheel robots have been proposed. The biologically inspired hexapod runner, Whegs [4], and the quadruped Mini Whegs [5], can climb obstacles 1.5 times as tall as their wheel radius, using rimless three-spoke wheels. RHex uses six semicircular legged wheels and an open-loop control system to climb steps of various heights [6]. The intelligent mobility platform with active spoke system uses three independently actuated spokes, each of which can change its length, which allows the wheel to climb over obstacles 1.7 times as tall as itself [7]. However, because the radius of a legged-wheel's rotation is inconsistent, the robot's center of mass oscillates vertically. Whegs and RHex both employ a tripod gait to minimize energy consumption [4], [6].

On the other hand, locomotion systems that can alternate between leg and wheel modes have been developed to take advantage of both systems. AZIMUT displays all the advantages of the leg, track, and wheel modes, and selects the optimal system for a given terrain [8]. Roller Walker can actively change the angles of the wheels mounted at the end of its legs, thereby allowing it to switch from leg mode to roller-skate mode [9]. The platform for ambulating wheels robot can reposition and lock its wheels to change from wheel mode to leg mode [10]. PEOPLER-II uses four wheels, each of which has two bars that allow the robot to walk on the ground in leg mode [11]. STAR can change its sprawl angles to crawl in different posture [25]. Furthermore, a mechanism that transforms wheels into legs has also been suggested. The rolling disk-biped robot can walk using two legs, which can transform into wheels [12]. The retractable wheel-leg module is able to transform into a leg with three-linkage systems [13]. Quattroped use active transformable wheels that can be converted into semicircles similar to those of RHex [14]. The deformable wheel can choose its driving mode between circular wheel, caterpillar, and legged wheel, using SMA actuators [26]. Origami wheel spreads its spokes when the wheel deforms using its origami structure [27]. However, these wheel-leg hybrid systems require additional actuators to switch between the two modes. As a result, the structure of the system becomes intricate, the control strategy is complicated, and the manufacturing cost increases.

The overall size of a robot places a constraint on the number of actuators that can be used in the system. Therefore, the design

Manuscript received February 27, 2014; revised September 5, 2014; accepted July 7, 2014. Date of publication November 20, 2014; date of current version December 3, 2014. This paper was recommended for publication by Associate Editor S. Kim and Editor B. J. Nelson upon evaluation of this reviewer's comments. This research was supported by a grant to Bio-Mimetic Robot Research Center, funded by Defense Acquisition Program Administration under the grant number UD130070ID.

Y. S. Kim, H. Kim, and C. N. Chu are with the Precision Engineering and Manufacturing Laboratory, School of Mechanical and Aerospace Engineering/Institute of Advanced Machines and Design, Seoul National University, 1 Gwanak-ro, Gwanak-gu, Seoul 151-742, Korea. (e-mail: yooseokteam@gmail.com; khn86@snu.ac.kr; cnchu@snu.ac.kr)

G. P. Jung and K. J. Cho are with the Biorobotics Laboratory, School of Mechanical and Aerospace Engineering/Institute of Advanced Machines and Design, Seoul National University, 1 Gwanak-ro, Gwanak-gu, Seoul 151-742, Korea. (e-mail: gwangpiljung@gmail.com; kjcho@snu.ac.kr)

This paper has supplementary downloadable material available at <http://ieeexplore.ieee.org>, provided by the author. The material consists of a video. This video illustrates the performance of a new type of wheel-leg hybrid robot, Wheel Transformer. This robot utilizes a novel transformable wheel that combines the advantages of both circular and legged wheels.

The transformation process of the wheel is passive, which eliminates the need for additional actuators. With the new transformable wheel, the robot can climb over an obstacle 3.25 times as tall as its wheel radius.

Color versions of one or more of the figures in this paper are available online at <http://ieeexplore.ieee.org>.

Digital Object Identifier 10.1109/TRO.2014.2365651



Fig. 1. New type of transformable wheel and Wheel Transformer.

of a small robot must minimize the number of actuators. Moreover, a less-complicated structure provides additional benefits, such as simpler control methods and lower manufacturing costs. Small robots are particularly advantageous in SAR missions, in which the utilization of swarm robotic systems would save time and increase efficiency [15]. The simplicity of a robot’s design significantly influences its control and performance in such situations, and even its manufacturing process. For these reasons, it is critical to devise a system that is simple, while still allowing a small robot to take advantage of both its wheels and legs.

We have developed a new type of transformable wheel (see Fig. 1), which was originally introduced at the 2013 IEEE International Conference on Robotics and Automation [16]. We have further improved the wheel by incorporating a new triggering mechanism and design optimization for better performance. Basically, it offers the advantages of both circular and legged wheels. In addition, it remains stable and energy efficient when driving on the even ground in its circular configuration. When it encounters an obstacle, the wheel transforms into a legged wheel with three legs. The change from the circular to the legged configuration is completed using only the frictional force between the wheel and obstacle without the need for additional actuators. The original design featured a foot with a rotating ankle joint that is used to trigger the transformation into a legged wheel. The design parameters of the wheel are tuned to maximize its climbing ability. Moreover, the wheel-leg hybrid robot, Wheel Transformer, is designed based on this wheel, and its design parameters are also tuned to enhance the abilities of the transformable wheel.

In the following sections, we will explain the design of the transformable wheel in more detail. We will then describe the optimization of the design parameters required to achieve better performance. We will also present the simple robot having transformable wheels, Wheel Transformer, and tune its design parameters to achieve stable climbing. Finally, we will conclude

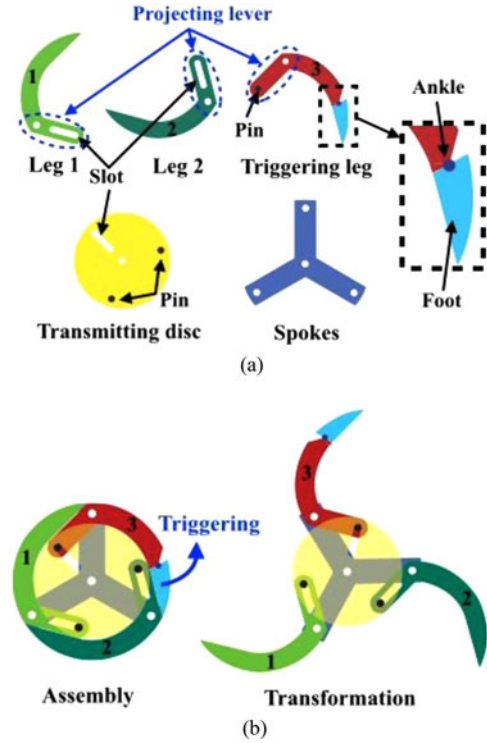


Fig. 2. Features of the new type of transformable wheel. (a) Five components. (b) Assembly and transformation into a legged wheel.

with a discussion of the performance improvement realized by our development.

II. DESIGN OF TRANSFORMABLE WHEEL

A. Component Design for Coupled Legs

The basic idea behind the new type of transformable wheel is to segment the rim into a number of legs and allow each leg to rotate about a revolute joint at the end of each spoke, as shown in Fig. 1. The number of segmented legs is the same as the number of the spokes. Furthermore, because all the legs must open passively on contact with no additional actuators, a transmitting disc is used to couple the opening of the legs.

Fig. 2(a) shows the five components of the transformable wheel: legs 1 and 2, the triggering leg, the transmitting disc, and the spokes. The spokes join the hub of the wheel to the segmented legs. The legs have a projecting lever with either a pin or slot, one of the legs acts as the triggering leg with a pin that rotates the transmitting disc, and the pins in the transmitting disc rotate the other two legs. The transmitting disc has two pins and a slot, 120° apart, which form pin-slot linkages with the legs. The triggering leg contains a foot with a rotating ankle joint at its end. Fig. 2(b) shows the assembled wheel and its transformation.

The transformable wheel should be capable of successfully transforming despite being presented with only a low level of friction. As explained in our previous research, when all three legs have the pins on their projecting levers to transform the wheel, the torque necessary for transformation is significantly increased [16]. This is because the slots on the transmitting disc have to rotate the pins on legs 1 and 2 during transformation,

TABLE I
NOMENCLATURE IN (1)–(12)

$F1_x$	Frictional force at the contact point with the ground ($= \mu F1_y$)
$F1_y$	Vertical reaction force at the contact point with the ground
$F2_x$	Normal reaction force at the contact point with the wall of an obstacle
$F2_y$	Frictional force at the contact point with the wall of an obstacle ($= \mu F2_x$)
$F3_x$	Frictional force at the treading point ($= \mu F3_y$)
$F3_y$	Vertical reaction force at the treading point
t	Time
θ	Angular displacement of the wheel ($= \omega t - \theta_0$) (θ_0 indicates the initial condition: before treading = 120° , after treading = 60°)
λ	Angular displacement of the triggering leg ($= \omega t - \lambda_0$) (λ_0 indicates the initial condition = 90°)
ω	Angular velocity of the wheel
α	Angular acceleration of the wheel
a	Linear acceleration of the wheel (subscript indicates directions.)
m	Mass of the robot
I	Moment of inertia of the robot
g	Gravitational acceleration
r	Radius of the circular wheel
μ	Friction factor
T_{T-Leg}	The torque at the revolute joint of the triggering leg
D_{pivot}	Pivot distance, the horizontal distance between the revolute joint of the triggering leg and the treading point

but the slot cannot rotate the pin in the pin-slot linkages of transformable wheel. Therefore, we arranged one pin on the triggering leg and the others on the transmitting disc to reduce the torque necessary for the transformation.

B. Triggering Mechanism

The success of transformation from a circular wheel into a legged wheel depends on the treading point of the triggering leg. When the triggering leg treads on the ground near the corner of an obstacle, the wheel readily transforms without difficulties. However, if the triggering leg treads on a surface below the wheel's center, the transformation does not occur because the mass of the robot hinders the legs from opening. In this section, we will show how a new triggering mechanism increases the probability of transformation in comparison with the transformable wheel without a triggering mechanism. We assume that the wheel quasi-statically rotates because of its slow and constant speed. All the variables in (1)–(12) are explained in Table I.

Fig. 3(a) depicts the moment when the triggering leg (indicated as leg 3) starts to contact the wall of an obstacle, as the wheel rotates at a uniform angular velocity ω . As shown in the free body diagram (FBD), the torque at the revolute joint of the triggering leg T_{T-Leg} is generated by the frictional force $F2_y$. The dynamic equations for the wheel are

$$F1_x - F2_x = ma_x \quad (1)$$

$$F1_y + F2_y - mg = ma_y \quad (2)$$

$$T_{T-Leg} = F2_y r (1 - \cos(\theta)) - F2_x r \sin(\theta). \quad (3)$$

The accelerations in both horizontal and vertical directions are zero, since the wheel neither proceeds nor climbs due to the

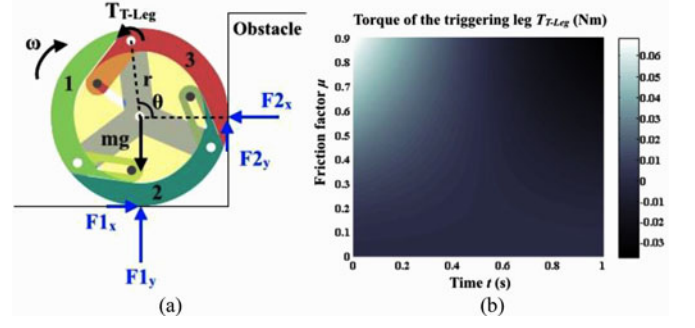


Fig. 3. Schematic diagrams depicting the moment when the triggering leg starting to contact an obstacle. (a) FBD of the transformable wheel. (b) Simulation result of the torque at the revolute joint of the triggering leg T_{T-Leg} .

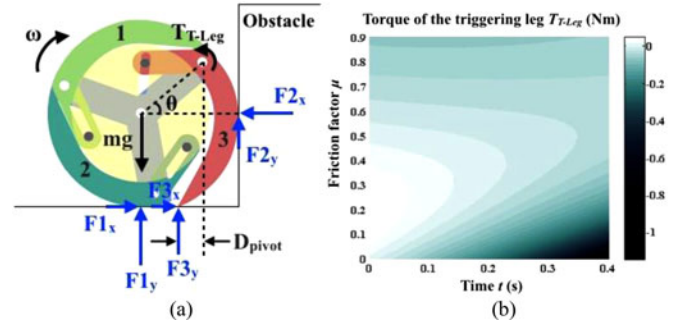


Fig. 4. Schematic diagrams depicting the transformation failure without the foot mechanism. (a) FBD of the transformable wheel without a foot. (b) Simulation result of the torque at the revolute joint of the triggering leg T_{T-Leg} .

obstacle. Substituting (1) and (2) into (3) yields T_{T-Leg} as

$$T_{T-Leg} = \frac{\mu mgr}{(\mu^2 + 1)} (\mu(1 - \cos(\theta)) - \sin(\theta)). \quad (4)$$

Fig. 3(b) shows the simulation result of T_{T-Leg} . As we expected, T_{T-Leg} is generated in the counterclockwise direction and increases as friction factor increases. As T_{T-Leg} is increased, the triggering leg more readily treads on the ground near the corner of the obstacle.

As the wheel continues to rotate, the triggering leg steps on the ground. Fig. 4(a) shows the FBD for the wheel and the triggering leg treading on the ground below the center of the wheel. In this case, the treading point is placed left to the revolute joint of the triggering leg. The torque at the revolute joint of the triggering leg T_{T-Leg} is generated by the reaction forces, and friction forces at the treading point and contact point with the wall of an obstacle. The dynamic equations for the wheel are derived as

$$F1_x + F3_x - F2_x = ma_x \quad (5)$$

$$F1_y + F2_y + F3_y - mg = ma_y \quad (6)$$

$$F1_x r + F2_y r + F3_x r + F3_y (r \cos(\theta)) + D_{pivot} - T_m = I\alpha \quad (7)$$

$$T_{T-Leg} = F3_x r (1 + \sin(\theta)) + F3_y D_{pivot} - F2_x r \sin(\theta) + F2_y r (1 - \cos(\theta)). \quad (8)$$

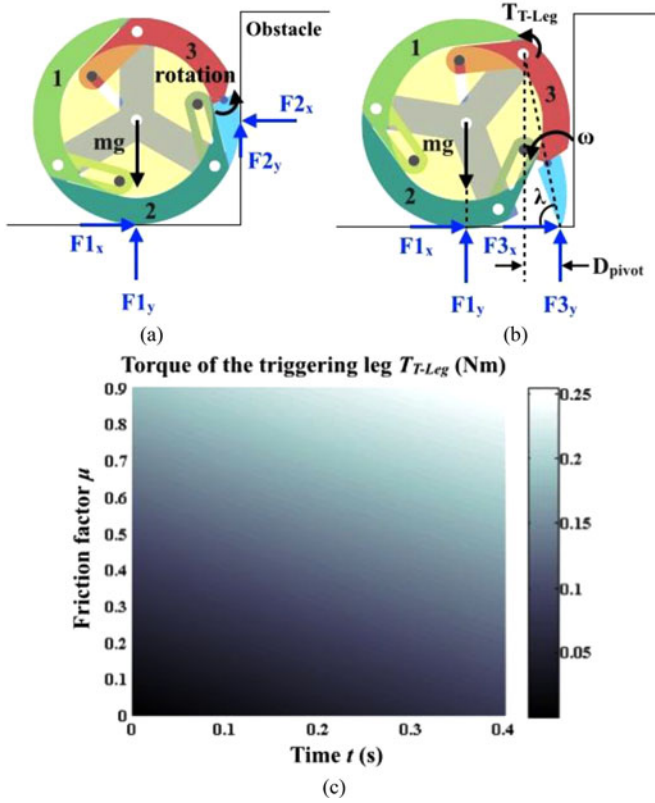


Fig. 5. Schematic diagrams depicting the triggering mechanism of a transformable wheel with a foot. (a) Foot rotates owing to friction. (b) Foot treads near the corner of an obstacle. (c) Simulation result of the torque at the revolute joint of the triggering leg T_{T-Leg} .

The accelerations in both horizontal and vertical directions are zero. The angular acceleration is also zero because the wheel rotates at the uniform angular velocity. The torque T_{T-Leg} is expressed as a function of time by substituting (5)–(7) into (8). Fig. 4(b) is the simulation result, which shows that T_{T-Leg} is generated in the clockwise direction regardless of the value of the friction factor. Therefore, T_{T-Leg} cannot transform the wheel because it closes the triggering leg. To change the direction of T_1 , we added a foot with a rotating ankle joint at the end of the triggering leg.

Fig. 5 shows how the foot is used to open the triggering leg, by generating a triggering torque in the counterclockwise direction. As shown in Fig. 5(a), the friction force between the foot and an obstacle causes the foot to rotate in the counterclockwise direction with respect to the ankle joint. The foot protrudes from the circumference of the wheel, and as the wheel continues to rotate, the foot approaches the corner of an obstacle and becomes planted. The torque T_{T-Leg} is generated in the counterclockwise direction due to the normal and friction forces at the treading point of the triggering leg; then, the triggering leg rotates about the treading point in the counterclockwise direction. Fig. 5(b) illustrates the FBD of the entire system, and the dynamic equations are given as

$$F1_x + F3_x < 0 \quad (9)$$

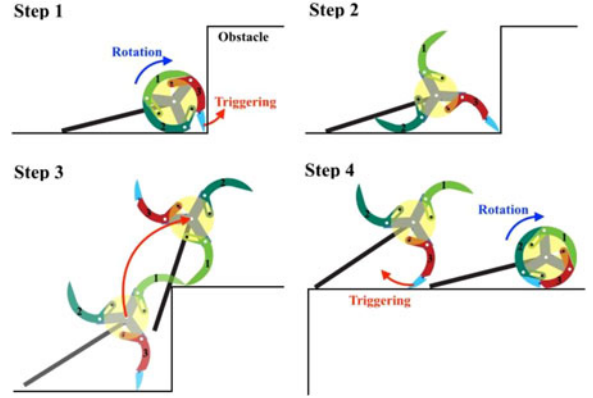


Fig. 6. Schematic diagrams illustrating the climbing scenario. In this scenario, the maximum height of an obstacle that the transformable wheel can climb over is taller than the wheel's radius.

$$F1_y + F3_y - mg = ma_y \quad (10)$$

$$T_{T-Leg} = \sqrt{3}r(F3_x \sin(\lambda) + F3_y \cos(\lambda)). \quad (11)$$

The vertical acceleration is zero as in previous cases, but the horizontal acceleration has the negative sign since the wheel recedes from the obstacle. Substituting (9) and (10) into (11) yields the following inequality:

$$T_{T-Leg} > \frac{\sqrt{3}}{2}mgr(\mu \sin(\lambda) + \cos(\lambda)). \quad (12)$$

Fig. 5(c) shows the simulation result of (12). When the foot is accompanied by the rotating ankle joint and is planted right to its revolute joint (near the corner of an obstacle), T_{T-Leg} is generated in the counterclockwise direction regardless of the value of the friction factor, which opens the triggering leg. Moreover, as we expected, T_{T-Leg} becomes greater as the friction factor increases.

To sum up, the success or failure of transformation is entirely determined by where the treading point of the triggering leg is located. If the triggering leg steps on the ground left to its revolute joint, transformation hardly occurs. If, however, the triggering leg treads on the ground right to its revolute joint, or near the corner of an obstacle, transformation is readily initiated. The friction factor can affect the probability that the triggering leg treads near the corner of an obstacle, but cannot convert the sign of T_{T-Leg} . Therefore, we used a foot with a rotating ankle joint to generate the torque necessary to trigger the transformation in the counterclockwise direction, which is not affected by the friction factor.

C. Climbing Scenario

When the transformation is initiated by the frictional force generated by the contact between the wheel and the wall of an obstacle, the transformable wheel can climb over an obstacle taller than the radius of the circular wheel. Fig. 6 illustrates how the transformable wheel climbs over an obstacle. In Step 1, the frictional force with the obstacle causes the triggering leg's foot to protrude from the circumference, which forms a point of support on the ground at the corner of the obstacle. In Step 2, as the

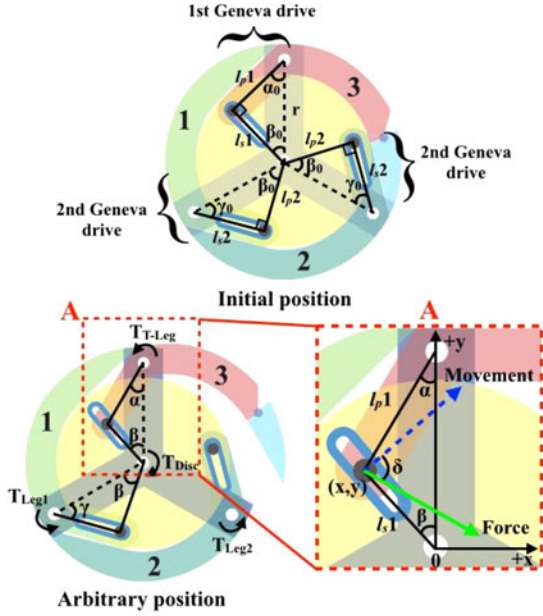


Fig. 7. Serial Geneva drives structure in the transformable wheel.

motor continues to revolve, the wheel rotates, but the supporting point does not move, such that the wheel transforms into a legged wheel. In Step 3, leg 1, following the triggering leg, treads on the upper surface of the obstacle. This treading point then becomes the axis of the robot's rotation, and the wheel climbs up and over the obstacle by rotating about the treading point. In Step 4, the robot's weight forces the wheel to fold back into a circle when the triggering leg is directly below the center of the wheel.

III. DESIGN OPTIMIZATION

This section describes the tuning of the initial design of the transformable wheel to achieve a high-transformation success rate. The torque necessary for transformation is minimized by tuning the wheel's design parameters in order to facilitate the transformation with even a low level of friction. The geometries of the foot are also tuned, such that the transformation occurs with a 100% success rate regardless of the wheel's angular velocity.

A. Modeling of Transformable Wheel

The quasi-static modeling of the transformable wheel should be derived prior to the tuning of the design parameters because the torque necessary for transformation T_{T-Leg} should not be increased by the optimization process. To this end, T_{T-Leg} is analyzed by modeling the transformable wheel.

Fig. 7 shows serial Geneva drives structure [28] in the transformable wheel. The first Geneva drive links the triggering leg with the transmitting disc, and the second Geneva drive links the transmitting disc with either leg 1 or 2. The angular displacements of the triggering leg, transmitting disc, and leg 1 or 2 are expressed α , β , and γ , respectively. To derive T_{T-Leg} , the angular acceleration of γ is derived as

$$\frac{d^2\gamma}{dt^2} = \frac{d^2\beta}{dt^2} \left(\frac{M_2 \cos(\beta) - 1}{1 + M_2^2 - 2M_2 \cos(\alpha)} \right)$$

$$+ \left(\frac{d\beta^2}{dt} \right) \frac{M_2(1 - M_2^2) \sin(\beta)}{(1 + M_2 - 2M_2 \cos(\beta))^2}. \quad (13)$$

However, to eliminate other variables except the time t in (13), the following equations are derived:

$$\alpha = \omega t - \alpha_0 \quad (14)$$

$$\beta = \tan^{-1} \left(\frac{\sin(\alpha)}{M_1 - \cos(\alpha)} \right) \quad (15)$$

$$\gamma = \tan^{-1} \left(\frac{\sin(\beta)}{M_2 - \cos(\beta)} \right) \quad (16)$$

$$M_1 = r/l_{p1} = 1/\cos(\alpha_0) \quad (17)$$

$$M_2 = r/l_{p2} = 1/\cos(\beta_0). \quad (18)$$

M_1 and M_2 are coefficients, and α_0 and β_0 indicate the initial values of α and β , respectively. The moment arm of the pin is expressed as l_p . As we assumed in Section II-B, the triggering leg rotates at the uniform angular velocity ω .

On the other hand, Fig. 7 also shows both the circular form of the transformable wheel before transformation, and an arbitrary state during transformation. In the enlarged view of part "A," the coordinates of the pin (x, y) can be expressed as

$$(x, y) = (-r \cos(\alpha_0) \sin(\alpha), r - r \cos(\alpha_0) \cos(\alpha)). \quad (19)$$

The directions of the slot's movement and the force on the pin are labeled with dotted and solid arrows, respectively. The tangent value of the angle between the two arrows δ is

$$\tan(\delta) = \frac{\cos(\alpha_0) \sin(2\alpha) - \sin(\alpha)}{\cos(\alpha) - \cos(\alpha_0) \cos(2\alpha)}. \quad (20)$$

The relationship between the torque at the center of transmitting disc T_{Disc} and T_{T-Leg} can be expressed as

$$T_{Disc} = T_{T-Leg} \frac{l_s 1}{l_p 1} \frac{1}{\sqrt{1 + \left(\frac{\cos(\alpha_0) \sin(2\alpha) - \sin(\alpha)}{\cos(\alpha) - \cos(\alpha_0) \cos(2\alpha)} \right)^2}} \quad (21)$$

where l_s is the moment arm of the slot. The identical process on the second Geneva drive also yields

$$T_{Leg1,2} = T_{T-Leg} \frac{1}{2} \frac{l_s 1}{l_p 1} \frac{l_s 2}{l_p 2} \frac{1}{\sqrt{1 + \left(\frac{\cos(\alpha_0) \sin(2\alpha) - \sin(\alpha)}{\cos(\alpha) - \cos(\alpha_0) \cos(2\alpha)} \right)^2}} \cdot \frac{1}{\sqrt{1 + \left(\frac{\cos(\beta_0) \sin(2\beta) - \sin(\beta)}{\cos(\beta) - \cos(\beta_0) \cos(2\beta)} \right)^2}} = I_{Leg1,2} \frac{d^2\gamma}{dt^2} \quad (22)$$

where $I_{Leg1,2}$ indicates the moment of inertia of leg 1 or 2, both of which have identical value with the other [16]. Since l_p and l_s in (22) are related to α and β , the following equation is derived

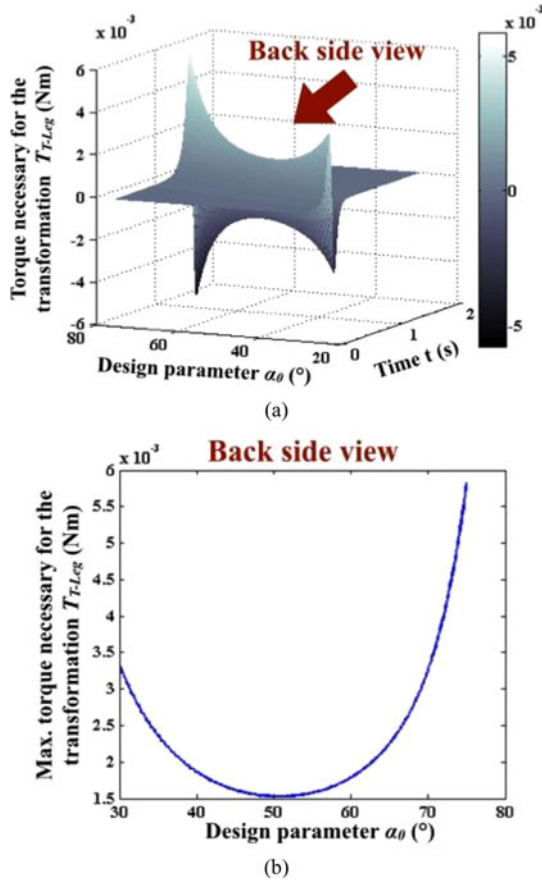


Fig. 8. (a) Simulation result of the triggering torque at the revolute joint of the triggering leg T_{T-Leg} . (b) Maximum value of (a) in the back-side view.

by geometrical analyses:

$$\frac{l_s 1 l_s 2}{l_p 1 l_p 2} = \frac{\sqrt{\cos^2(\alpha_0) \sin(2\alpha) - \sin(\alpha)}}{\cos(\alpha_0)} \cdot \frac{\sqrt{\cos^2(\beta_0) \sin(2\beta) - \sin(\beta)}}{\cos(\beta_0)}. \quad (23)$$

Substituting (13) and (23) into (22) yields T_{T-Leg} in terms of the design parameter α_0 and variable t , and the simulation result of T_{T-Leg} is shown in Fig. 8(a). The value of T_{T-Leg} peaks near the middle phase of transformation, which is a typical characteristic of the Geneva drive [28]. Fig. 8(b) also shows the back-side view of Fig. 8(a), which plots the maximum value of T_{T-Leg} as a function of α_0 during transformation. The maximum of T_{T-Leg} has the lowest value of 15×10^{-3} N·m at $\alpha_0 = 50$.

On the other hand, the maximum height of an obstacle that the wheel can climb over is affected by the transformation ratio, which is the ratio between the radii before and after the transformation. In Fig. 9(a), a geometric interpretation of the transformation ratio gives

$$\frac{R}{r} = \sqrt{4 - 2\sqrt{3} \cos\left(2\alpha_0 + \frac{\pi}{6}\right)} \quad (24)$$

where R is the distance between the center of the wheel and the end of each leg of the legged wheel. As shown in Fig. 9(b), the transformation ratio is completely dependent on α_0 , and reaches

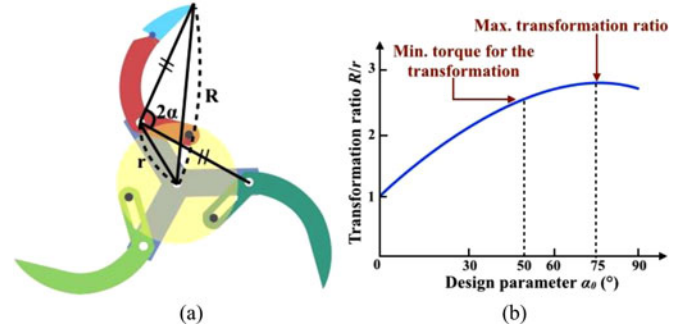


Fig. 9. (a) Transformation ratio is indicated as the ratio between radii before and after the transformation. (b) Graph of the transformation ratio. To minimize the torque for the transformation, 50° as the value of α_0 .

the maximum when $\alpha_0 = 75$. However, we could not choose 75° as the value of α_0 because it increases the triggering torque T_{T-Leg} to its maximal level. Moreover, α_0 is affected by the thickness of the legs and their projecting levers; the projecting levers can protrude from the circumference of the circular wheel when α_0 is 75° . Therefore, we chose 50° as the value of α_0 to minimize the torque necessary for transformation, as well as to maintain the circular shape of the wheel. This condition also allows the wheel to have a greater transformation ratio than our previous research [16].

B. Foot Design for High-Transformation Success Rate

As shown in Fig. 5, the torque at the revolute joint of the triggering leg is generated by reaction forces at the treading point. As the triggering leg treads on the ground as close to the corner of an obstacle as possible, the torque is increased. Therefore, we aimed to tune the design parameters of the foot for the desirable treading. On the other hand, after the transformation, if the wheel rotates at high speed, the wheel cannot stably climb over the obstacle owing to the repulsive force generated by the impact of the rotating legs on the upper surface of the obstacle. Therefore, we also aimed to tune the foot design parameters to transform the wheel at low speeds.

In Fig. 10(a), the length of the foot that allows the foot to tread the corner of an obstacle is geometrically analyzed, and can be found from the following condition:

$$L_f \sin(\varphi) \geq (\sqrt{2} - 1)r + \frac{t}{2} \quad (25)$$

where L_f is the length of the foot, φ is the angular displacement of the foot's rotation, and t is the thickness of the leg. Before choosing values for the parameters from (25), boundary condition for L_f was established. Fig. 10(b) shows the graph of (25), which indicates that L_f cannot be lower than 21 mm. On the other hand, when the foot continued to contact with the wall of an obstacle after its rotation, normal reaction force of the wall closed the foot; the foot should lose the contact with the wall after opening. Therefore, L_f should be as short as possible. Boundary condition for φ was also established. The larger the angular displacement, the thinner triggering leg becomes, which may cause the destruction of the leg, while it receives the repulsive forces from the ground in the

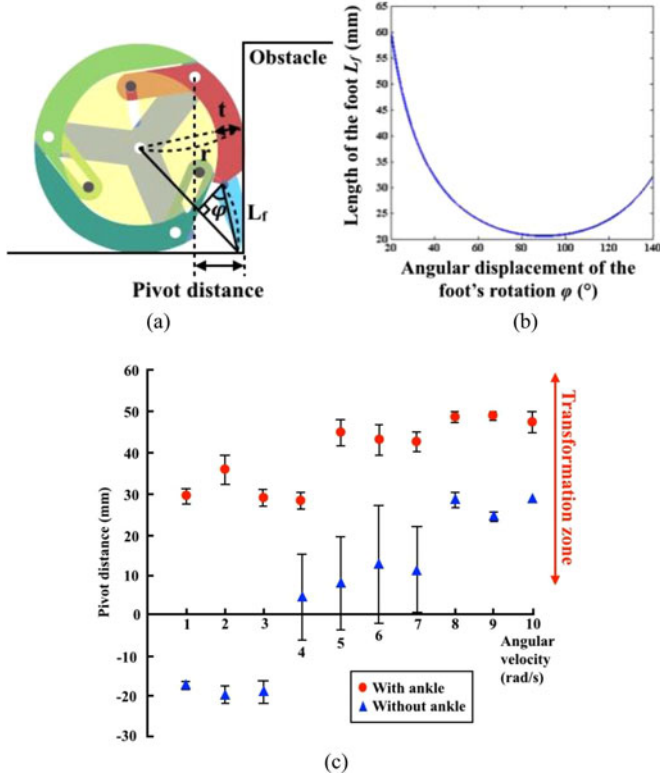


Fig. 10. Design optimization of the foot to increase the pivot distance. (a) Parameters for the foot design. (b) Boundary condition for the foot design. (c) With a foot, the pivot distance is usually above 30 mm, which is sufficient to transform the circular wheel into a legged wheel regardless of the wheel's angular velocity.

legged-wheel mode driving. The chosen values were determined to be $L_f = 23.5$ mm and $\varphi = 60^\circ$, while $r = 40$ mm and $t = 8$ mm. The efficacy of the foot was tested at least three times on a raised platform with each angular velocity condition, as shown in Fig. 10(a). Fig 10(c) shows the relationship between the pivot distance and the angular velocity of the wheel, both with and without the foot. Empirically, the transformation occurred when the pivot distance was greater than 10 mm. As expected, the pivot distance increased when the wheel incorporated a foot, which allowed the triggering leg to open on contact with the obstacle regardless of its angular velocity. Without this foot, however, the wheel was unable to transform at angular velocities of 1 to 3 rad/s. For angular velocities of 4, 5, 6, and 7 rad/s, the success rate of the transformation was 50%, 67%, 75%, and 75%, respectively, and 100% for 8 rad/s and up. As the angular velocity increases, the motor's torque also increases; thus, raising the normal force of the triggering leg acting on the wall of the obstacle. As a result of the increased friction force between the triggering leg and wall, the triggering leg rotated around its revolute joint and trod on the ground near the obstacle. In this case, however, the robot could not stably climb over the obstacle owing to the excessive repulsive forces resulting from the impact of the rotating legs on the ground. Therefore, we can say that the foot should be used to facilitate the transformation, even at low speeds.

On comparing the experimental results with analytical results, we derived the angular displacement of the triggering leg

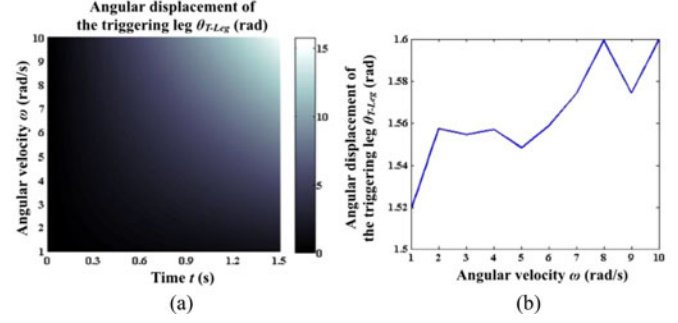


Fig. 11. (a) Analytical result of the angular displacement of the triggering leg. (b) Time it took the triggering leg from contacting an obstacle to treading on the ground is estimated at each angular velocity condition, and the θ_{T-Leg} values from (a) are plotted.

θ_{T-Leg} by double integration of the angular acceleration of the triggering leg derived from (4), and we estimated the relationship between D_{pivot} and ω for the indirect comparison with experimental results. From (4), θ_{T-Leg} is derived as

$$\theta_{T-Leg} = \frac{\mu mgr}{I_{T-Leg}(\mu^2 + 1)} \left(\mu \left(\frac{t^2}{2} + \frac{\cos(\theta)}{\omega^2} \right) + \frac{\sin(\theta)}{\omega^2} \right) + C_1 t + C_2. \quad (26)$$

The moment of inertia of the triggering leg is expressed as I_{T-Leg} . The integral constants C_1 and C_2 are given as

$$C_1 = \omega - \frac{\mu mgr(\mu \sin(\theta_0) - \cos(\theta_0))}{I_{T-Leg} \omega(\mu^2 + 1)} \quad (27)$$

$$C_2 = -\frac{\mu mgr(\mu \cos(\theta_0) + \sin(\theta_0))}{I_{T-Leg} \omega^2(\mu^2 + 1)}. \quad (28)$$

Fig. 11(a) shows the simulation result of (26). As seen in this graph, θ_{T-Leg} increases as the wheel rotates faster. We estimated the time it took the triggering leg from contacting an obstacle to treading on the ground at each angular velocity, and plotted θ_{T-Leg} at each condition [see Fig. 11(b)]. A larger angular displacement means a longer pivot distance. Furthermore, by employing the foot with the rotating ankle, the plotted values becomes vertically shifted upward as illustrated in the experimental results of Fig. 10(c).

IV. DESIGN OF ROBOTIC PLATFORM

This section describes the design of a wheel-leg hybrid robot called Wheel Transformer, which was intended to evaluate the performance of the new type of transformable wheel (see Figs. 1 and 12). To achieve stable obstacle climbing, the body length and the motor's angular velocity are tuned to reduce slippage at the point of contact between the legs and obstacle.

A. Features

Some previously developed robots were able to climb over obstacles taller than the radius of their wheels by using linkage systems, such as a rocker bogie mechanism [17]–[20]. However, such systems are not suitable for small mobile robots because of their large size. In contrast, Wheel Transformer uses only the

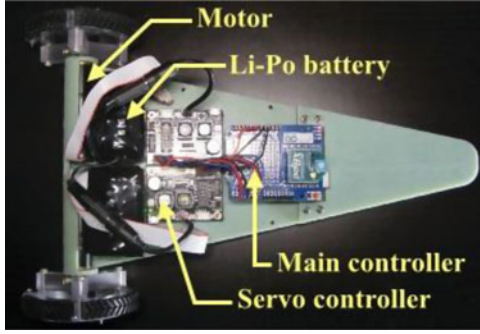


Fig. 12. Wheel Transformer features.

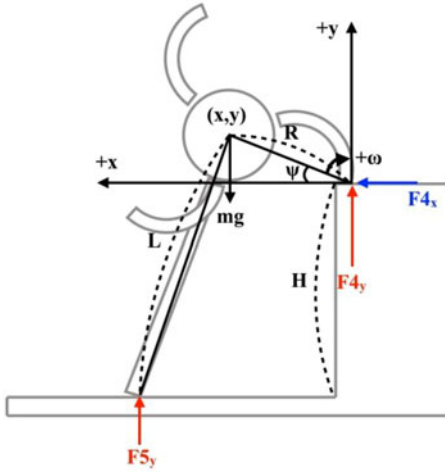


Fig. 13. FBD of Wheel Transformer climbing onto a raised platform.

two transformable wheels to test the new wheel's applicability to small mobile robots. To minimize any energy loss caused by a transmission system, each wheel was attached directly to the motor's axis. Steering was achieved by independently rotating both wheels (differential steering).

The electronics consisted of two servo controllers for each of the two motors used in the robot. When the DC motors are controlled by pulse width modulation, a lower voltage is applied to achieve lower speeds; thereby, resulting in a lower torque. When climbing over an obstacle, the motors must rotate slowly to minimize the repulsive forces caused by the legs striking the obstacle; however, a high torque is required to lift the robot over the obstacle. The servo controller allows the motor to produce a high torque at low speeds. The main controller uses an XBee to communicate wirelessly with a computer, as well as issues digital signals to the servo controller.

B. Tuning Design Parameters for Stable Climbing

To enable the robot to climb over an obstacle, the stepping leg must be at the center of rotation and must not slip. Fig. 13 shows the FBD of Wheel Transformer climbing onto a raised platform. The greater the normal force at point F_{4y} is, the more stable the robot can climb over an obstacle. As shown in Fig. 13, coordinates (x, y) describe a circular motion, the center of which is at the end of the leg and radius R . The angular speed is kept

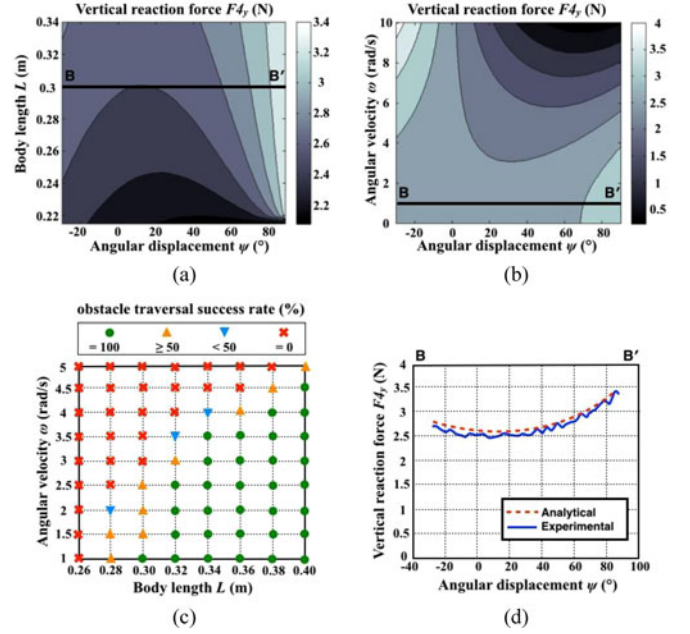


Fig. 14. Analytical and experimental results for the normal force as a function of rotational angle of leg (ψ). (a) Body length (L) at $\omega = 1$ rad/s is the design parameter. (b) Angular velocity of the motor (ω) at $L = 0.3$ m is the design parameter. (c) The results of climbing test of Wheel Transformer. (d) 2-D graph of intercept B–B' in (a) and (b).

constant by the servo controllers. Thus, the dynamic equations for coordinates (x, y) are

$$F_{4x} = -mR\omega^2 \cos(\psi) \quad (29)$$

$$F_{4y} + F_{5y} - mg = -mR\omega^2 \sin(\psi) \quad (30)$$

$$F_{4x}R \sin(\psi) - F_{4y}R \cos(\psi) + F_{5y}\sqrt{L^2 - (H + R \sin(\psi))^2} = 0 \quad (31)$$

where F_x , F_y , H , L , ω , and ψ indicate the horizontal and vertical reaction forces, height of the raised platform, length of the robot's body, angular velocity of the motor, and angular displacement of the stepping leg, respectively. Substituting (29) and (30) into (31) yields F_{4y} as

$$F_{4y} = \frac{m \left(g - R\omega^2 \sin(\psi) - \frac{R^2 \omega^2 \sin(\psi) \cos(\psi)}{\sqrt{L^2 - (H + R \sin(\psi))^2}} \right)}{1 + \frac{R \cos(\psi)}{\sqrt{L^2 - (H + R \sin(\psi))^2}}} \quad (32)$$

The simulation was run for $H = 130$ mm, $m = 0.7$ kg, and $R = 85$ mm, with L and ω as the design parameters. Fig. 14(a) represents F_{4y} with respect to changes in L and ψ at $\omega = 1$ rad/s. As L increases, the normal force also increases; thereby, allowing the robot to stably climb over the obstacle. The reason for this is that as L increases, F_{5y} becomes further away from the center of mass, which increases the portion of the weight supported by F_{4y} . Fig. 14(b) represents F_{4y} with respect to changes in ω and ψ at $L = 0.3$ m. When the value of ψ varies from -30° to 90° , as ω increases, the normal force decreases because as the velocity of the leg stepping onto the top surface of

TABLE II
PHYSICAL SPECIFICATIONS OF TRANSFORMABLE WHEEL
AND WHEEL TRANSFORMER

Transformable wheel	
Circular wheel radius	40 mm
Legged-wheel radius	85 mm
Transformation ratio	212.5%
Max. obstacle height	150 mm
Weight	63 g
Material	Polycarbonate and rubber pad (Misumi Corp.)
Wheel Transformer	
Size	210 mm × 340 mm × 80 mm (width × length × height)
Weight	700 g
Motors	Maxon dc motor (4.5 W; 16 mm dia.) × 2 Rated voltage: 12 V Rated torque: 4.26 m-Nm Rated current: 0.569 A Max. speed: 16 000 r/min
Gearheads	Maxon 84:1 planetary gearhead × 2
Encoders	Maxon 512 CPT encoder × 2
Servo controllers	Escon 36/2 dc servo controller × 2
Main controller	Arduino Uno R3 with Xbee module
Batteries	Li-Po battery × 2 (14.8 V, 1400 mAh per pack)

the obstacle increases, the repulsive force of the leg striking the surface increases. The climbing ability of Wheel Transformer was tested ten times at each condition with the 130-mm-tall raised platform, and the results are presented in Fig. 14(c). A 100% obstacle traverse success rate is expressed as a circle. Specifically, Wheel Transformer was able to stably surmount the raised platform with no slippage when $L \geq 0.3$ m. We chose 0.3 m as the robot body length for a small and compact robot size; thus, ω was set at 1 rad/s. The value of F^4_y at $L = 0.3$ m and $\omega = 1$ rad/s are shown, respectively, as cross sections labeled B–B' in Fig. 14(a) and (b). These values are shown as a 2-D plot with a dotted line in Fig. 14(d). The solid line represents experimental values obtained using a load cell (capacity: 1 kgf, resolution: 0.05 gf, CASKOREA), and approximates to the values obtained by the simulation. Errors are caused by the difference between the assumed and actual situation, i.e., any slight off-centeredness of the robot's center of mass relative to the wheel's center. Combined with the results shown in Fig. 10(c), it was found that both easy transformation and stable climbing were possible at $\omega = 1$ rad/s.

V. RESULTS

The new type of transformable wheel and Wheel Transformer were fabricated based on the analyses described in Sections II–IV (see Fig. 1). The physical specifications are elaborated in Table II. The transformable wheel and Wheel Transformer were created using a CNC milling machine and a 3-D printer, respectively.

The transformable wheel incorporates the functional advantages of both circular and legged wheels. Specifically, when the wheel is in its circular configuration, the robot displays stable

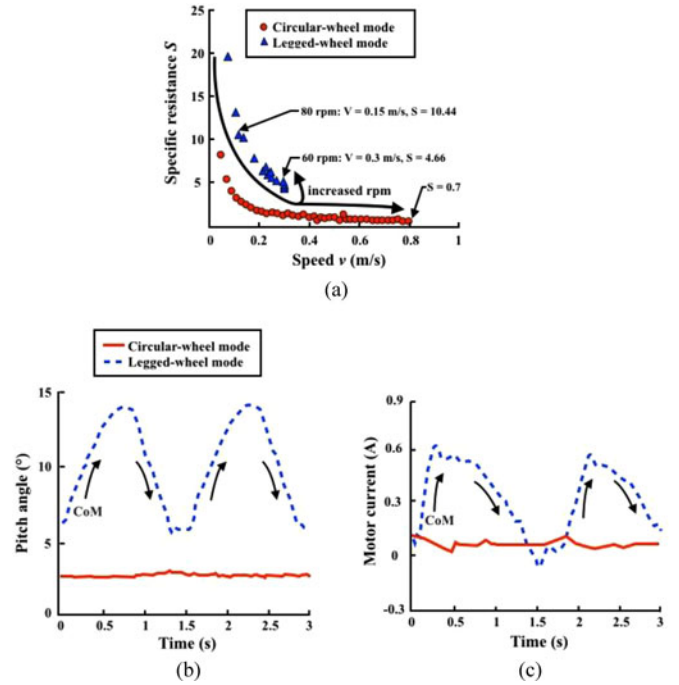


Fig. 15. Performance evaluation for the circular-wheel mode: (a) Specific resistance. (b) Pitch angles of the robot. (c) Electric current consumption of each motor.

and efficient driving performance on flat surfaces with no oscillation of its center of mass. When the wheel transforms into the legged wheel, on the other hand, it attains the ability to climb over obstacles taller than the wheel radius. In this section, we evaluate the performance in each mode.

A. Speed and Specific Resistance

In a typical circular-wheel mode, the distance between the center of the wheel and the point of contact with the ground, i.e., the wheel's radius remains constant, which makes it possible for the robot to move stably and efficiently with no vertical oscillation. While the robot can maintain stable contact with the ground, the motor can propel it so that its forward speed increases. Accordingly, the speed of the robot is proportional to its driving stability. The efficiency of the robot is evaluated based on its specific resistance S [21]

$$S = \frac{P(v)}{mgv} \quad (33)$$

where $P(v)$ and v refer to the total power consumption rate of the battery and speed of the robot, respectively. Figs. 15(a)–(c) shows the specific resistance on flat surfaces, pitch angle of the robot, and the electric current consumption of the motor in the circular wheel and legged-wheel modes, respectively. These lead us to the following three conclusions.

- 1) As shown in Fig. 15(a), in circular-wheel mode, the robot's speed reaches a maximum of 0.8 m/s (2.4 body lengths per second, the upper limit of the motor). With the legged wheels, however, it did not exceed 0.3 m/s. Increasing the angular velocity of the motor, as indicated by the arrows

in Fig. 15(a), consequentially increases the repulsive force generated when the leg strikes the ground. As the robot bounces, the normal force decreases. Thus, in the legged-wheel mode, the robot cannot gain extra speed because of the decrease in friction. When the motor rotated at 60 r/min, the speed of the robot was 0.3 m/s, and the specific resistance was 4.66. When the motor rotated at 80 r/min, however, the speed of the robot was 0.15 m/s, and the specific resistance was 10.44. For this case, the robot was unable to move faster, even if the motor rotated faster than 80 r/min.

- 2) Because the center of the robot's mass oscillates vertically, the legged wheels have a greater specific resistance [see Fig. 15(a)]. As shown in Fig. 15(b), the pitch angles of the robot in the legged-wheel mode were plotted on a sinusoidal curve with a constant amplitude and period, whereas the pitch angles of the robot in circular-wheel mode remained almost constant. These results suggest that the center of the robot's mass moved up and down as the motor rotated because the wheel's radius of rotation was not constant. Therefore, more electric current was consumed when the center of the robot's mass moved upward, as shown in Fig. 15(c). The mean current consumption is 0.3 A in the legged-wheel mode, which is significantly higher than the 0.07 A drawn in circular-wheel mode for the same rotational speed (10 r/min). Mini Whegs and RHex, with their four- and six-legged wheels, achieve lower energy consumptions by decreasing the amplitude of the center of the mass displacement curve by adopting a diagonal and tripod walking gaits, respectively [5], [6]. Wheel Transformer, however, demonstrates relatively high energy consumption in legged-wheel mode given that it has only two transformable wheels.
- 3) As depicted on the inverse proportion curve shown in Fig. 15(a), the specific resistance decreases, as the speed increases in the circular-wheel mode because the speed increases at a higher rate than the power consumption. The specific resistance is 0.7 at 0.8 m/s in the circular-wheel mode, which is comparable to that of previously developed robots at the same speed (Quattroped: 0.5 [14], Roller Walker: 0.7 [22], Scout II: 2.4 [23]).

The specific resistance varies depending on whether the electric current is consumed solely by the motors or by the entire robot [22]. Most robots that use wheel-leg hybrid locomotion adopt additional actuators for switching modes along with the actuators that are essential to the robot's locomotion; thus, varying the specific resistance. On the other hand, Wheel Transformer has only two motors to operate the transformable wheels with no additional actuators. The current consumption of the actuators is thus nearly equal to that of the entire robot. Consequently, the adoption of a more efficient motor would lower the specific resistance.

B. Obstacle Climbing

The improved climbing ability in the legged-wheel mode is shown in Fig. 16(a)–(c), which shows that the robot can climb

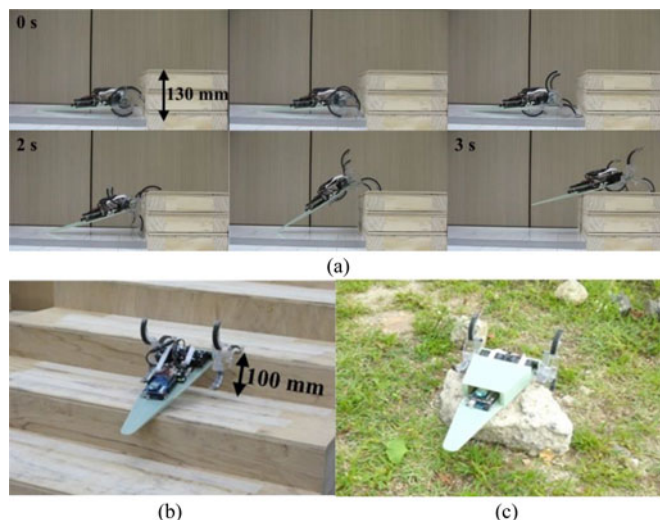


Fig. 16. Performance evaluation for the legged-wheel mode. (a) Raised platform climbing. (b) Staircase climbing. (c) Natural terrain traversing.

up onto a raised platform, climb a staircase, and climb a stone in natural rough terrain, a neither of which would be possible in circular-wheel mode. The angular velocity was set at 1 rad/s to ease the transformation process and minimize the slippage of the legs during climbing, as described in Sections III and IV.

The obstacle shown in Fig. 15(a) is a 130-mm-tall raised platform, which is 3.25 times and 1.53 times as tall as the circular and legged wheel's radii, respectively. The body of Wheel Transformer was designed to easily climb over a 130-mm-tall obstacle with a 100% success rate. With taller obstacles, however, the legs would slip and not be able to pull the center of mass up over the corner of the obstacle. On the other hand, the legged wheel could place its leg on top of platforms as tall as 150 mm. When only one of the triggering legs came into contact with the obstacle and the legged wheel placed its leg on the top of the obstacle before the other one did, the robot body would tilt laterally, making it impossible for the other legged wheel to place its leg on the obstacle. This problem stems from the phase difference between the two triggering legs, which calls for further research into phase sensing.

Fig. 16(b) shows Wheel Transformer climbing a staircase, in which each riser is 100 mm high. Quattroped with its four-legged wheels, as well as RHex and Whegs with their six-legged wheels are able to climb stairs without slipping by relying on propulsion from their rear wheels [4], [6], [14]. Although Wheel Transformer has less forward propulsion, because of it having only two-legged wheels, it offers the advantage of not requiring control of the phase between the front and rear wheels [24].

Fig. 16(c) shows Wheel Transformer traversing stones in natural rough terrain. Since one of the most important applications of the transformable wheel is SAR missions, its capability of negotiating natural rough terrain should be verified. Unlike the raised platform and staircase, the irregular and uneven faces of stones are not vertical to the ground, and the trajectory of the robot cannot be perpendicular to the wall of a stone.

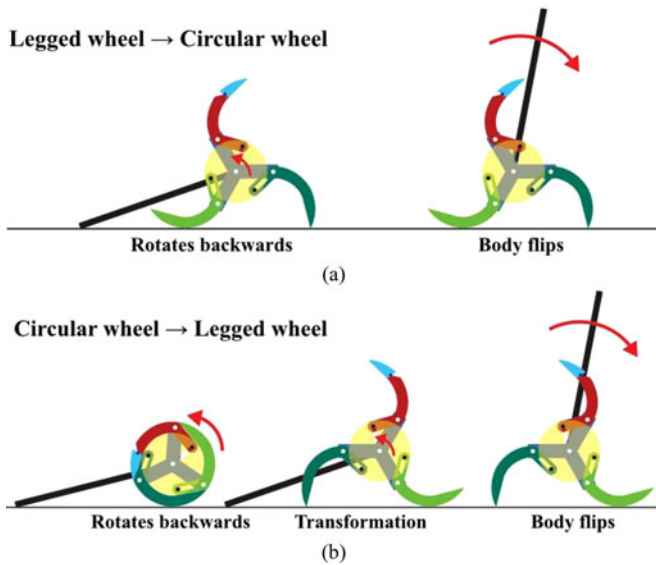


Fig. 17. Mode switching (a) from the legged wheel into the circular wheel (b) from the circular wheel into the legged wheel.

Despite these difficulties, Wheel Transformer successfully traversed stones with an 80% success rate out of five trials.

C. Discussion of Mode Switching

A new kind of transformable wheel was developed to combine the advantages of both circular wheels and legged wheels. On a flat surface, the wheel should maintain its circular shape for better driving performance. However, when the wheel rotated clockwise at a rate in excess of 4.2 rad/s on a flat surface, the centrifugal force caused the legs to rotate counterclockwise about their revolute joints. The legs would also open if the foot got caught in small crevices in the ground. When, on the other hand, the wheel rotated counterclockwise, it was unable to transform because the legs should rotate counterclockwise about their revolute joints for the transformation, while the robot's mass hindered the transformation. Therefore, to achieve high-speed locomotion with circular wheels, the directions of wheel's and legs' rotation must be the same. Of course, if the wheel were to rotate counterclockwise without flipping the body, the body would hinder the robot's locomotion by becoming caught by any rough terrain. In order to prevent this from happening, the body was designed to be flipped over the wheels and the robot had to make a U-turn whenever the robot switched its driving mode from the legged wheel into the circular wheel.

Wheel Transformer is able to flip the body using the same two dc motors that are used for the robot's locomotion. As illustrated in Fig. 17(a), in legged-wheel mode, the torque required to back up the robot is greater than the torque required to flip the body over because the robot's center of mass is located near the wheel's center. If, therefore, motor rotates backward, the wheel will remain stationary, and the body will flip over the wheels as a result of relative motion. In circular-wheel mode, if the wheel

rotates backward quickly, it transforms into the legged wheel via the centrifugal force, and the body flips over due to the relative motion [see Fig. 17(b)].

VI. CONCLUSION

In this study, we developed a new type of transformable wheel that offers the strengths of both circular and legged wheels, i.e., the stable and energy-efficient driving ability of circular wheels, and the obstacle climbing ability of legged wheels. The five components were designed for the coupled-leg system of the transformable wheel. The design parameters of the wheel were adjusted to maximize the transformation ratio and enable the transformation of the wheel at low speeds. Wheel Transformer was discussed in terms of its features, and its design parameters were tuned to enable stable climbing.

Wheel Transformer achieved a speed of 2.4 body lengths per second with a specific resistance of 0.7 and an ability to climb over obstacle of 130 mm in height, which is 3.25 times as tall as the radius of its circular wheel. Because Wheel Transformer uses only two dc motors for its locomotion, steering, and the transformation of the wheels, it would be possible to increase its agility and lower the specific resistance simply by improving the motor capabilities. Future works in this study may include controlling the phases of the triggering leg, while climbing so that the transformation of both wheels occurs simultaneously; thus, preventing the body from tilting laterally.

A new type of transformable wheel was developed for small mobile robots that could be applied to SAR missions. Specifically, the wheel's size can be reduced because of the simplicity of the design that allows transformation without the use of additional actuators. In addition, this compact design would simplify the control strategy as well as lower the manufacturing costs; thereby, allowing its application to swarm robotic systems. This would increase the mission success rate.

REFERENCES

- [1] D. F. Hougen, S. Benjaafar, J. C. Bonney, J. R. Budenske, M. Dvorak, M. Gini, H. French, D. G. Krantz, P. Y. Li, and F. Malver, "A miniature robotic system for reconnaissance and surveillance," in *Proc. IEEE Int. Conf. Robot. Autom.*, 2000, pp. 501–507.
- [2] F. Matsuno and S. Tadokoro, "Rescue robots and systems in Japan," in *Proc. IEEE Int. Conf. Robot. Biomimetics*, 2004, pp. 12–20.
- [3] M. Kaspari and M. D. Weiser, "The size-grain hypothesis and interspecific scaling in ants," *Funct. Ecol.*, vol. 13, no. 4, pp. 530–538, 1999.
- [4] R. D. Quinn, J. T. Offi, D. A. Kingsley, and R. E. Ritzmann, "Improved mobility through abstracted biological principles," in *Proc. IEEE/RSJ Int. Conf. Intell. Robots Syst.*, 2002, pp. 2652–2657.
- [5] J. M. Morrey, B. Lambrecht, A. D. Horchler, R. E. Ritzmann, and R. D. Quinn, "Highly mobile and robust small quadruped robots," in *Proc. IEEE/RSJ Int. Conf. Intell. Robots Syst.*, 2003, pp. 82–87.
- [6] U. Saranlı, M. Buehler, and D. E. Koditschek, "RHex: A simple and highly mobile hexapod robot," *Int. J. Robot. Res.*, vol. 20, no. 7, pp. 616–631, Jul. 2001.
- [7] J. B. Jeans and D. Hong, "IMPASS: Intelligent mobility platform with active spoke system," in *Proc. IEEE Int. Conf. Robot. Autom.*, 2009, pp. 1605–1606.
- [8] F. Michaud, D. Létourneau, M. Arseneault, Y. Bergeron, R. Cadrin, F. Gagnon, M.-A. Legault, M. Millette, J.-F. Paré, and M.-C. Tremblay, "Multi-modal locomotion robotic platform using leg-track-wheel articulations," *Auton. Robots*, vol. 18, no. 2, pp. 137–156, 2005.

- [9] S. Hirose, "Variable constraint mechanism and its application for design of mobile robots," *Int. J. Robot. Res.*, vol. 19, no. 11, pp. 1126–1138, Nov. 2000.
- [10] J. A. Smith, I. Sharf, and M. Trentini, "PAW: A hybrid wheeled-leg robot," in *Proc. IEEE Int. Conf. Robot. Autom.*, 2006, pp. 4043–4048.
- [11] T. Okada, W. T. Botelho, and T. Shimizu, "Motion analysis with experimental verification of the hybrid robot PEOPLER-II for reversible switch between walk and roll on demand," *Int. J. Robot. Res.*, vol. 29, no. 9, pp. 1199–1221, Aug. 2010.
- [12] C. C. Phipps, B. E. Shores, and M. A. Minor, "Design and quasi-static locomotion analysis of the rolling disk biped hybrid robot," *IEEE Trans. Robot.*, vol. 24, no. 6, pp. 1302–1314, Dec. 2008.
- [13] K. Tadakuma, R. Tadakuma, A. Maruyama, E. Rohmer, K. Nagatani, K. Yoshida, A. Ming, M. Shimojo, M. Higashimori, and M. Kaneko, "Mechanical design of the wheel-leg hybrid mobile robot to realize a large wheel diameter," in *Proc. IEEE/RSJ Int. Conf. Intell. Robots Syst.*, 2010, pp. 3358–3365.
- [14] S. C. Chen, K. J. Huang, W. H. Chen, S. Y. Shen, C. H. Li, and P. C. Lin, "Quattroped: A leg-wheel transformable robot," *IEEE/ASME Trans. Mechatronics*, vol. 19, no. 2, pp. 730–742, Apr. 2013.
- [15] D. P. Stormont, "Autonomous rescue robot swarms for first responders," in *Proc. IEEE Int. Conf. Comput. Intell. Homeland Security Pers. Safety*, 2005, pp. 151–157.
- [16] Y. S. Kim, G. P. Jung, H. Kim, K. J. Cho, and C. N. Chu, "Wheel transformer: A miniaturized terrain adaptive robot with passively transformed wheels," in *Proc. IEEE Int. Conf. Robot. Autom.*, 2013, pp. 5625–5630.
- [17] C. Grand, F. Benamar, F. Plumet, and P. Bidaud, "Stability and traction optimization of a reconfigurable wheel-legged robot," *Int. J. Robot. Res.*, vol. 23, nos. 10/11, pp. 1041–1058, Oct./Nov. 2004.
- [18] P. S. Schenker, T. L. Huntsberger, P. Pirjanian, E. T. Baumgartner, and E. Tunstel, "Planetary rover developments supporting mars exploration, sample return and future human-robotic colonization," *Auton. Robots*, vol. 14, nos. 2/3, pp. 103–126, 2003.
- [19] T. Estier, Y. Crausaz, B. Merminod, M. Lauria, R. Piguat, and R. Siegwart, "An innovative space rover with extended climbing abilities," in *Proc. Space Robot.*, 2000, pp. 333–339.
- [20] G. Quaglia, D. Maffiolo, W. Franco, S. Appendino, and R. Oderio, "The Epi-q-1 hybrid mobile robot," *Int. J. Robot. Res.*, vol. 29, no. 1, pp. 81–91, Jan. 2010.
- [21] T. Von Karman and G. Gabrielli, "What price speed? Specific power required for propulsion of vehicles," *Mech. Eng.*, vol. 72, pp. 775–781, 1950.
- [22] G. Endo and S. Hirose, "Study on roller-walker: Energy efficiency of roller-walk," in *Proc. IEEE Int. Conf. Robot. Autom.*, 2011, pp. 5050–5055.
- [23] I. Poulakakis, "Modeling and experiments of untethered quadrupedal running with a bounding gait: The Scout II robot," *Int. J. Robot. Res.*, vol. 24, no. 4, pp. 239–256, Apr. 2005.
- [24] S. C. Chen, K. J. Huang, C. H. Li, and P. C. Lin, "Trajectory planning for stair climbing in the leg-wheel hybrid mobile robot quattroped," in *Proc. IEEE Int. Conf. Robot. Autom.*, 2011, pp. 1229–1234.
- [25] D. Zarrouk, A. Pullin, N. Kohut, and R. S. Fearing, "STAR, a sprawl tuned autonomous robot," in *Proc. IEEE Int. Conf. Robot. Autom.*, 2013, pp. 20–25.
- [26] D. Y. Lee, J. S. Koh, J. S. Kim, and K. J. Cho, "Deformable-wheel robot based on soft material," *Int. J. Precision Eng. Manuf.*, vol. 14, no. 8, pp. 1439–1445, 2013.
- [27] D. Y. Lee, J. S. Kim, J. J. Park, S. R. Kim, and K. J. Cho, "Fabrication on origami wheel using pattern embedded fabric and its application to a deformable mobile robot," in *Proc. IEEE Int. Conf. Robot. Autom.*, 2014, p. 2565.
- [28] R. O. Pamley, "Geneva wheel design," in *Illustrated Sourcebook of Mechanical Components*, 1st ed., New York, NY, USA: McGraw-Hill, 2000, ch. 1, pp. 34–35.



Yoo-Seok Kim (S'12) received the B.S. degree in mechanical engineering from Korea University, Seoul, Korea, in 2012. He is currently working toward the M.S. degree at the School of Mechanical and Aerospace Engineering, Seoul National University, Seoul.

His research interests include novel mechanism design and the fabrication of biologically inspired robots, and also computer-aided manufacturing and precision machining.



Gwang-Pil Jung (S'11) received the B.S. degree in mechanical engineering from Korea Advanced Institute of Science and Technology, Daejeon, Korea, in 2010. He is currently working toward the Ph.D. degree in mechanical engineering at the Biorobotics Laboratory, Seoul National University, Seoul, Korea.

His research interests include the design and fabrication of biologically inspired robots and novel mechanisms using smart materials, structures, and actuators.

Mr. Jung received a 2013 IROS Best Video Award.



Haan Kim received the B.S. degree from the School of Mechanical and Aerospace Engineering, Seoul National University, Seoul, Korea, in 2010, where he is currently working toward the Ph.D. degree.

His research interests include the mechanism design of microrobot and actuators, and also in nontraditional precision machining of smart materials.



Kyu-Jin Cho (M'08) received the B.S. and M.S. degrees from Seoul National University, Seoul, Korea, in 1998 and 2000, respectively, and the Ph.D. degree in mechanical engineering from Massachusetts Institute of Technology, Cambridge, MA, USA, in 2007.

He was a Postdoctoral Fellow with Harvard Microrobotics Laboratory until 2008. At present, he is an associate professor of Mechanical and Aerospace Engineering and the director of Biorobotics Laboratory at Seoul National University.

His research interests include biologically inspired robotics, soft robotics, soft wearable robots, and rehabilitation/ assistive robotics. He received the 2014 IEEE RAS Early Academic Career Award, 2014 ASME Compliant Mechanism Award, and 2013 IROS Best Video Award.



Chong-Nam Chu received the B.S. degree in mechanical engineering from Seoul National University, Seoul, Korea, in 1979, and the M.S. and Ph.D. degrees in mechanical engineering from Massachusetts Institute of Technology, Cambridge, MA, USA, in 1982 and 1986, respectively.

From 1986 to 1992, he was a Professor with the School of Industrial Engineering, Purdue University, West Lafayette, IN, USA, and a Visiting Scientist with the Institute of Physical and Chemical Research and Institute of Industrial Science, University of Tokyo, Tokyo, Japan, in 1990. He is currently a Professor with the School of Mechanical and Aerospace Engineering, Seoul National University. His research interests include computer-aided manufacturing, precision machining, micromachining, and motion, and force-feedback control.